Ceramide Synthase 4 Regulates Stem Cell Homeostasis and Hair Follicle Cycling

Franziska Peters[1,2,3], Susanne Vorhagen[2,4], Susanne Brodesser[1,2], Kristin Jakobshagen[1], Jens C. Brüning[2,3,5,6,7], Carien M. Niessen[2,3,4] and Martin Krönke[1,2,3]

Ceramides are crucial for skin barrier function, but little is known about the regulation of epidermal appendages and whether stem cell populations that control their regeneration depend on specific ceramide species. Here we demonstrate that ceramide synthase 4 (CerS4) is highly expressed in the epidermis of adult mice where it is localized in the interfollicular epidermis and defined populations within the pilosebaceous unit. Inactivation of CerS4 in mice resulted in precocious activation of hair follicle bulge stem cells while expanding the Lrig1$^+$ junctional zone and sebaceous glands. This was preceded first by a decrease in bone morphogenetic protein (BMP) and a subsequent increase in Wnt signaling. This imbalance in quiescent versus activating signals likely promoted a prolonged anagen-like hair follicle state after the second catagen, which exhausted stem cells over time ultimately resulting in hair loss in aged mice. K14-Cre-mediated deletion of CerS4 revealed a similar phenotype, thus suggesting an epidermis intrinsic function of CerS4 in regulating the regeneration of the pilosebaceous unit. The data indicate that CerS4-directed epidermal ceramide composition is essential to control hair follicle stem and progenitor cell behavior potentially through its regulation of BMP and Wnt signaling.

Journal of Investigative Dermatology (2015) **135,** 1501–1509; doi:10.1038/jid.2015.60; published online 26 March 2015

[1]*Institute for Medical Microbiology, Immunology and Hygiene, University of Cologne, Cologne, Germany;* [2]*Cologne Excellence Cluster on Cellular Stress Responses in Aging Associated Diseases (CECAD), Cologne, Germany;* [3]*Center for Molecular Medicine Cologne (CMMC), Cologne, Germany;* [4]*Department of Dermatology, University of Cologne, Cologne, Germany;* [5]*Institute for Genetics, University of Cologne, Cologne, Germany;* [6]*Center for Endocrinology, Diabetes and Preventive Medicine, University of Cologne, Cologne, Germany and* [7]*Max Planck Institute for Neurological Research, Cologne, Germany*

Correspondence: Carien M Niessen, Cologne Excellence Cluster on Cellular Stress Responses in Aging Associated Diseases (CECAD) or Center for Molecular Medicine Cologne (CMMC) or Department of Dermatology, University of Cologne, Joseph-Stelzmann-Strasse 26, 50931 Cologne, Germany or Martin Krönke, Institute for Medical Microbiology, Immunology and Hygiene or Cologne Excellence Cluster on Cellular Stress Responses in Aging Associated Diseases (CECAD) or Center for Molecular Medicine Cologne (CMMC), University of Cologne, Goldenfelsstrasse 19-21, 50935 Cologne, Germany.
E-mail: carien.niessen@uni-koeln.de or m.kroenke@uni-koeln.de

FP, SV, SB, KJ, CMN, and MK designed experiments and/or analyzed the data. MK and JCB initiated the study. FP, SV, SB, and KJ performed the experiments. FP, CMN, and MK wrote the paper. All authors read the paper.

Abbreviations: BMP, bone morphogenetic protein; BrdU, bromodioxyuridine; CerS, ceramide synthase; CerS1-6, ceramide synthase 1-6; CoA, coenzyme A; Fatty acyl-chain of ceramides "hx:y": h, hydroxylated at α- or ω-position; x, number of carbon atom; y, number of double bonds; HF, hair follicle; HFSC, hair follicle stem cell; IFE, interfollicular epidermis; IRS, inner root sheath; JZ, junctional zone; K14, keratin 14; K15, keratin 15; LRC, label–retaining cell; Lrig1, leucine-rich repeats and immunoglobulin-like domains protein 1; MS, mass spectrometry; SC, stem cell; SG, sebaceous gland; P, postnatal; Sphingoid base of ceramides "dx:y": d, dihydroxy (hydroxylated with two OH groups), x, number of carbon atoms; y, number of double bonds.; Wnt, Wg for Wingless and Int for the Int-gene

Received 25 June 2014; revised 28 January 2015; accepted 8 February 2015; accepted article preview online 23 February 2015; published online 26 March 2015

INTRODUCTION

Ceramides are central components of mammalian membranes and key players in different signaling pathways (Pettus *et al.*, 2002). Ceramide production depends on ceramide synthases (CerS), consisting of six members (CerS1–6), which catalyze the third step of ceramide biosynthesis by acylating sphinganine to dihydroceramide using coenzyme A (CoA)-activated fatty acids. Furthermore, CerS also acylate sphingosine formed in the salvage pathway of sphingolipid degradation, leading directly to ceramide production (Levy and Futerman, 2010). In mammals, CerS1–6 have different substrate specificities and expression patterns. CerS4 shows a substrate preference for C18:0- to C26:0-CoA (Mizutani *et al.*, 2005), and CerS4 mRNA was ubiquitously expressed in mouse tissue with the strongest expression in skin (Laviad *et al.*, 2008; Schiffmann *et al.*, 2013; Ebel *et al.*, 2014), suggesting an essential role for CerS4 in skin biology.

The mammalian epidermis is a self-renewing stratified epithelium consisting of the interfollicular epidermis (IFE) and its appendages: sebaceous glands (SGs) and hair follicles (HFs). Epidermal renewal is maintained by distinct adult epidermal stem cell (SC) populations, which are located in the basal layer of the IFE and in specific localizations of the HF. The adult HF consists of an upper permanent part and a lower cycling portion that undergoes continuous phases of growth (anagen), apoptosis-driven regression (catagen), and rest (telogen) (Blanpain and Fuchs, 2009). The induction of anagen requires local activation of bulge hair follicle stem cells (HFSCs) (Greco *et al.*, 2009). HF cycling is regulated by a spatially and

temporally tightly controlled diverse set of signaling agonists and antagonists derived from the HF and its dermal niche (Plikus *et al.*, 2011; Fuchs and Chen, 2013).

Recently, Ebel *et al.* (2014) showed that CerS4 deficiency resulted in age-related hair loss and excess sebaceous lipid production. However, little is known whether CerS and ceramide composition regulate SC behavior and control formation and maintenance of epidermal appendages. Here we show that epidermal CerS4 is crucial for normal homeostasis of the pilosebaceous unit by regulating HF stem/progenitor cells.

RESULTS

CerS4 is expressed in the pilosebaceous unit

To characterize epidermal expression of CerS1–6, RNA was isolated from newborn (P0) and postnatal (P) day 16, 21, 25, 33, 47, and 58 epidermis. Western blot analysis revealed proper separation of the epidermis from the dermis (Supplementary Figure S1 online). Quantitative real-time (Qrt) PCR analysis revealed high expression of CerS3 mRNA in P0 and P21 mouse epidermis that was strongly reduced at later adult stages (Figure 1a). Expression of CerS2 and CerS6 mRNA was low, whereas CerS1 mRNA was not detectable (not shown). CerS4 and CerS5 were weakly expressed in P0 epidermis but showed a strong increase when cells entered telogen (P21), followed by a modest decrease in anagen (P25, P33), and a subsequent increase in catagen (P47), which was slightly reduced again in telogen (P58). CerS4 expression was still comparable in aged (P365) mice (Figure 1a). These data might suggest a functional role of CerS4 in adult epidermis.

Immunofluorescence analysis revealed that CerS4 was not only expressed in the IFE but also in HFs, showing a dynamic localization pattern during the HF cycle (Figures 1b and c, Supplementary Figure S2 online). In telogen HFs, CerS4^{+} cells were located at the lower part of the junctional zone (JZ) and in the isthmus/upper bulge region (arrow, Figure 1b left panel), which was further confirmed by co-staining with the bulge HFSC markers K15 or CD34 (Supplementary Figure S3 online). At P21, staining was also observed in the secondary hair germ (Supplementary Figure S2 online). In anagen, CerS4 was further detected in the inner root sheath (IRS) of the cycling part of the HF (arrow, Figure 1b). Occasionally, distinct sebocytes in the SGs stained positive for CerS4 (star, Figure 1b). Whole-mount staining and co-staining with Lrig1, a marker for JZ progenitors (Jensen *et al.*, 2009), further confirmed JZ and isthmus/upper bulge localization in telogen HFs and the IRS localization in anagen HFs (Figures 1c and d). Interestingly, whole-mount staining revealed single CerS4^{+} cells in the lower bulge that were only weakly positive for keratin 15 (K15) (Figure 1e,Supplementary Figure S3 online). However, CerS4 mRNA was not detectable in α6-integrin^{+}/CD34^{+} HFSCs (Figure 1f).

CerS4 inactivation results in a functional loss of CerS4 activity

To examine the functional significance of CerS4 in the epidermis, CerS4$^{-/-}$ mice were generated by introducing loxP sites flanking exon 3 of the *CerS4* gene and crossed with general deleter Cre-carrying mice (Schwenk *et al.*, 1995) (Supplementary Figure S4 online). CerS4 enzymatic activity was assessed in epidermal lysates using sphinganine-D7 as substrate. In the presence of C20:0-CoA for which CerS4 has the highest affinity, epidermal lysates of CerS4$^{-/-}$ mice produced significantly less D7-d18:0-ceramide-C20:0 and D7-d18:1-ceramide-C20:0 (Figure 2), indicating a functional loss of CerS4 activity.

Mass spectrometry analyses showed a decrease in non-hydroxylated ceramides with acyl-chain length of C20:0 and in hydroxylated ceramides with acyl-chain lengths of C22:0 in P0 CerS4$^{-/-}$ compared with CerS4$^{+/+}$ epidermis (Supplementary Figure S5a and b online). In P33 epidermis, a decrease of nonhydroxylated ceramide species with acyl-chain lengths of C18:0 and C20:0 was detected upon loss of CerS4, accompanied by an increase in nonhydroxylated ceramide species with acyl-chain lengths of C16:0 and C24:0 (Supplementary Figure S5d online). Similarly, a decrease in hydroxylated ceramide species with acyl-chain lengths of C18:0 and C20:0 was detected, along with an increase in hydroxylated ceramide species with acyl-chain lengths of C22:0 and C24:0 (Supplementary Figure S5e online).

In contrast, no differences in protein-bound ceramides were observed in P0 and P33 epidermis (Supplementary Figure S5c and f online). Thus, loss of CerS4 results in a decrease in long-chain ceramides, in line with previously published findings (Laviad *et al.*, 2008; Hartmann *et al.*, 2013; Ebel *et al.*, 2014).

Inactivation of CerS4 results in hair loss and altered homeostasis of epidermal appendages

CerS4$^{-/-}$ mice were born at Mendelian ratios with no obvious phenotype. Older CerS4$^{-/-}$ mice displayed a gradual hair loss spreading from the ventral toward the dorsal side (P220–P365, Figure 3a), with almost complete alopecia of the torso at 19 months of age (P585, Figure 3a).

To characterize how CerS4$^{-/-}$ mice lose their hair, we performed histological analysis of HFs. At P0 CerS4$^{-/-}$, mice did not show obvious differences in HF morphology (data not shown) and density (Figure 3c). The density of HFs decreases by P16, likely as a result of growth and expansion of the integument (Claxton, 1966). This decrease was much less pronounced in CerS4$^{-/-}$ back skin, and increased density remained at later P stages (P21, P33, P47, and P64) (Figures 3b and c). From P21 onward, a gradual increase in the width of the infundibulum and enlarged SGs were also observed in CerS4$^{-/-}$ mice (Figures 3b and d).

CerS4 is essential for HF cycling

Next, we assessed whether loss of CerS4 affects HF cycling. No obvious differences were observed in the ability of CerS4$^{-/-}$ HFs to enter catagen (data not shown), telogen (P21), or anagen (P33) in the first hair cycle. Similarly, no obvious changes were observed for the second catagen (P47) (Figures 3b and e). However, whereas CerS4$^{+/+}$ HFs were in telogen at P51, all CerS4$^{-/-}$ HFs showed an anagen-like morphology (Figures 3b and e). In addition, when CerS4$^{+/+}$ HFs remained in telogen (e.g., P58, P64, and P78, Figure 3b and Supplementary Figure S6 online), no telogen HFs were observed in CerS4$^{-/-}$ mice at these or later stages.

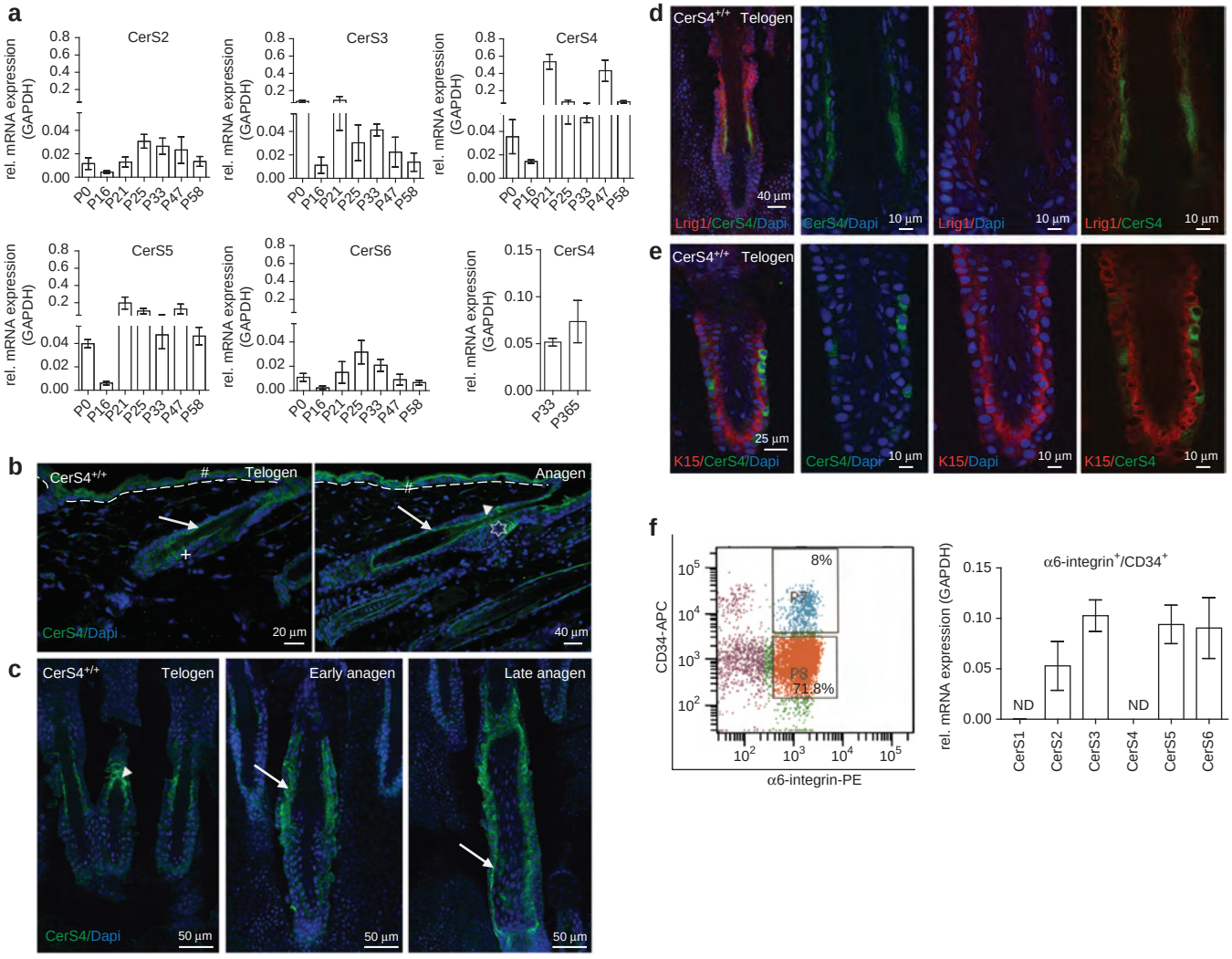

Figure 1. CerS4 is expressed in the hair follicle (HF). **(a)** QRT-PCR for CerS2-6 mRNA in epidermal splits. Mean ± SEM; $n > 3$ mice/genotype. (**b**) Immunofluorescence staining of CerS4 on cryo sections isolated from CerS4+/+ mice at P21 (telogen) and P33 (anagen). White arrows indicate CerS4 staining of IRS, + single CerS4$^+$ cells in bulge, # staining in IFE, arrow heads JZ staining, star single CerS4$^+$ cells in SG, and the dashed lines border between epidermis and dermis. (**c**) Immunofluorescence staining of CerS4 on tail whole mounts at P21 (telogen) and P33 (early and late anagen). Immunofluorescence staining of Lrig1 (**d**), K15 (**e**), and CerS4 on tail whole mounts at P58 (telogen). (**b**–**e**) Nuclei were counterstained with DAPI. (**f**) FACS-plot of α6-integrin$^+$/CD34$^+$ cells. QRT-PCR of CerS1–6 mRNA in FACS-sorted HFSCs. Mean ± SEM; $n > 3$ mice/genotype. DAPI, 4',6-diamidino-2-phenylindole; HFSC, hair follicle stem cell; IFE, interfollicular epidermis; IRS, inner root sheath; JZ, junctional zone; ND, not detectable; SG, sebaceous gland; QRT-PCR, quantitative real-time PCR.

Similar results were obtained in mice in which CerS4 was selectively deleted in the epidermis using K14-Cre (CerS4$^{epi\,-/-}$, Figure 3f), indicating that the observed phenotype is caused by an epidermis-intrinsic function of CerS4. These data show that after the second catagen CerS4$^{-/-}$ HFs were precociously activated to enter growth phase. Together, the data indicate that loss of CerS4 resulted in early P changes in HF and SG morphology and HF cycling that likely contribute to the later hair loss.

CerS4$^{-/-}$ affects HFSC quiescence

Precocious anagen entry, widened infundibulum, and enlarged SGs of CerS4$^{-/-}$ HFs might result from increased proliferation. Whereas short-term bromodioxyuridine (BrdU) labeling revealed no difference within HFs at P0, an increase in BrdU$^+$ cells in CerS4$^{-/-}$ HFs was observed at P16, and this difference persisted during the first telogen (P21), second anagen (P33), catagen (P47), and was still detectable after 6 months (P182) (Figures 4a and b).

Label–retaining experiments (Braun *et al.*, 2003) revealed a strong reduction (around 84%) in BrdU label–retaining bulge SCs (LRCs) of CerS4$^{-/-}$ mice at P70 (Figures 4c and d), indicating a loss of quiescent bulge SCs. This was accompanied by a reduction of the K15$^+$ bulge HFSC population at P70 (Figure 4e), suggesting that inappropriate activation of HFSCs is accompanied by SC loss. Precocious SC activation was further confirmed by shaving at P47, which resulted in accelerated anagen entry and earlier hair regrowth in CerS4$^{-/-}$ mice (Figure 4f).

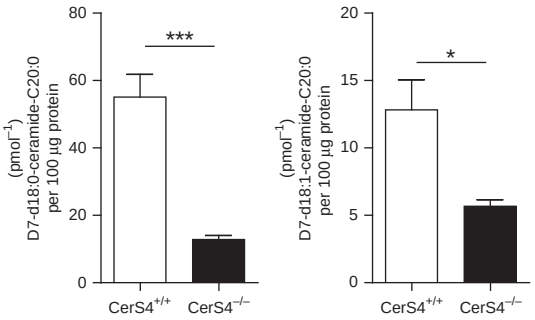

Figure 2. Functional reduction of CerS activity. Activity of CerS in epidermal lysates supplemented with deuterated D7-sphinganine as substrate and C20:0 acyl-CoA as cosubstrate. Dihydroceramide and ceramide consisting of deuterated C18-sphingosine and C18-sphinganine base and C20:0 fatty acid were quantified by Nano-ESI MS/MS. $*P<0.05$, $***P<0.005$. Nano-ESI MS/MS, electrospray ionization mass spectrometry.

CerS4$^{-/-}$ leads to reduced numbers of HFSCs and increase of JZ progenitor cells

HFs contain several spatially and functionally different populations of stem/progenitor cells (Blanpain and Fuchs, 2009); we therefore examined how loss of CerS4 would affect these populations. Whole-mount staining confirmed the reduction of K15$^+$ cells in the bulge (arrow, Figure 5a, Figure 4e). In line with this, FACS analysis revealed a significant reduction of α6-integrin$^+$/CD34$^+$ cells in CerS4$^{-/-}$ epidermis, already at P47, which was further reduced in 1-year-old CerS4$^{-/-}$ mice (P328–343, Figure 5c). In HFs, keratin 6 (K6) is expressed in the outer root sheath adjacent to the CerS4$^+$-IRS and in a CD34$^-$ population within the bulge that normally does not contribute to HF homeostasis (Hsu *et al.*, 2011). However, no obvious changes in K6 localization were observed, suggesting that loss of CerS4 did not affect this K6$^+$ population (Figure 5b). Interestingly, in CerS4$^{-/-}$ mice, Lrig1 staining was no longer restricted to the JZ but spread toward SGs (Figure 5d), indicating that these cells feed into the enlarged SGs. Staining of whole-mount HFs for SCD1, a marker for differentiated sebocytes, confirmed enlargement of SGs in CerS4$^{-/-}$ mice and revealed multiple lobules in these CerS4$^{-/-}$ SGs (dashed line, Figure 5e). Thus, CerS4 deficiency results in activation and reduction of HFSCs while expanding the Lrig1$^+$ progenitor cell population, which may explain the increase in SG size and lobules.

Imbalanced BMP and Wnt signaling in CerS4$^{-/-}$ mice

We next investigated whether loss of CerS4 would affect key signaling pathways that control HFSC activation and quiescence. We took P47 (catagen) epidermis, as our data indicated that CerS4$^{-/-}$ HFs were unable to undergo transition into the next telogen at P49. We examined Wnt/β-catenin and TGFβ signaling, as these promote activation of bulge SCs (Blanpain and Fuchs, 2009; Goldstein and Horsley, 2012) and BMP activity, which promotes entry into telogen and quiescence of bulge SCs (Plikus *et al.*, 2011). RT-PCR analysis revealed no significant differences in Wnt target gene expression, such as Axin2, Tcf3, Tcf4, or Wnt10b, at P47 (Figure 6a).

No differences were detected in the expression of shared TGFβ/BMP ligands and targets such as BMP-2,-4, Smad7, Id1, and Id2. In contrast, mRNA expression of BMP target genes Msx1 and Msx2 were reduced, indicating a decrease in BMP signaling in CerS4$^{-/-}$ P47 epidermis, shortly before entry into telogen. This may explain the inability of CerS4$^{-/-}$ HFSCs to subsequently enter telogen (Plikus *et al.*, 2008). Interestingly, at P58, a strong increase in the Wnt targets Axin2 (7-fold) and Wnt10b (8-fold) was found in CerS4$^{-/-}$ epidermis (Figure 6b), in line with the fact that BMP signaling counterbalances Wnt (Kandyba *et al.*, 2013), which then likely further promotes an anagen-like state. No significant differences in BMP/TGFβ pathway–related mRNA expression were observed at P58, albeit Msx2 mRNA was increased (Figure 6b), which might contribute to anagen maintenance (Alonso and Fuchs, 2006). As P58 CerS4$^{+/+}$ and CerS4$^{-/-}$ hair follicles were in different hair cycle stages, telogen versus anagen, we next compared CerS4$^{-/-}$ P58 anagen with P33 CerS4$^{+/+}$ anagen epidermis and detected similar levels of Wnt and BMP target gene expression. This indicates that at P58 CerS4$^{-/-}$ HFs resembled anagen HFs also from a signaling perspective (Supplementary Figure S7a online). Comparison of Msx2 and Wnt10b at different HF stages within either CerS4$^{+/+}$ or CerS4$^{-/-}$ epidermis visualized time-dependent mRNA expression (Supplementary Figure S7b and c online), further illustrating that altered signaling fluctuations correlate with a changed HF cycle.

DISCUSSION

Ceramides are crucial for skin barrier function (Jennemann *et al.*, 2012; Rabionet *et al.*, 2014), and loss of ceramides is observed in aging human skin (Imokawa *et al.*, 1991). However, little is known whether specific ceramides control skin appendage homeostasis. Here we show that CerS4 is a major CerS expressed in adult murine epidermis and appendages. CerS4 controls epidermal stem/progenitor cell homeostasis and HF cycling. Loss of CerS4 resulted in inappropriate activation of HFSCs, expansion of the HF JZ and enlarged SGs. These alterations are associated with decreased BMP in catagen followed by increased Wnt signaling. This signal imbalance likely leads to precocious HFSC activation to drive the continuous anagen-like state of CerS4$^{-/-}$ HFs and ultimately led to exhaustion of HFSCs and hair loss in older mice.

Our study identifies a previous unrecognized contribution of CerS4 and ceramides in the activation and maintenance of adult SCs. Sphingolipid metabolites were previously shown to regulate a plethora of cellular processes including cell growth, differentiation, and cell death (Maceyka and Spiegel, 2014). Notably, we did not observe any obvious difference in apoptosis (not shown). Instead, loss of CerS4 promoted an early increase in proliferation and activation of HFSCs.

BMP signaling promotes quiescence of the bulge SC population (Kobielak *et al.*, 2007) and counteracts β-catenin signaling in the bulge compartment by suppressing Wnt expression (Kandyba *et al.*, 2013). Thus, reduced BMP signaling in CerS4$^{-/-}$ mice may promote Wnt/β-catenin signaling that will then strongly stimulate activation of

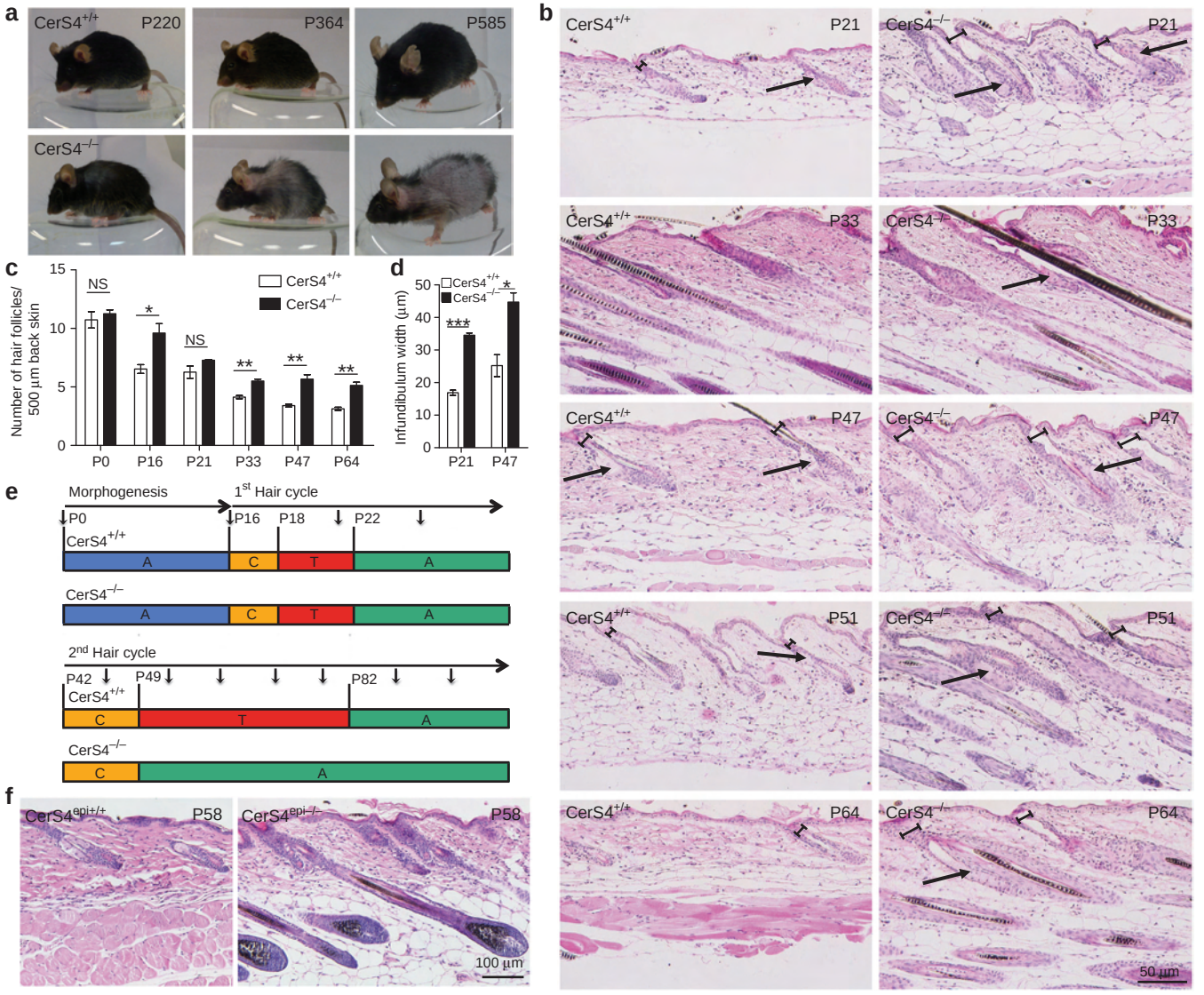

Figure 3. CerS4-dependent alteration in hair follicle (HF) morphology and cycling. **(a)** Macroscopic appearance of CerS4$^{+/+}$ and CerS4$^{-/-}$ littermates at indicated P days. **(b)** H&E-stained paraffin sections. Black arrows indicate increased SGs and black brackets indicate increased infundibulum width. **(c)** Quantification of HF density using H&E-stained sections. Mean ± SEM. $n \geq 3$ mice/genotype. *$P<0.05$; **$P<0.01$. **(d)** Quantification of infundibulum width using H&E-stained sections at indicated P days. Mean ± SEM. $n = 3$ mice/genotype. *$P<0.05$; ***$P<0.001$. **(e)** Schematic representation of hair cycle stages (small black arrows indicate P days at which mice were analyzed). Morphogenesis (A), blue; anagen (A), green; catagen (C), orange; telogen (T), red. HF cycle time is based upon C57BL/6 mice. **(f)** H&E-stained sections from CerS4$^{epi+/+}$ (CerS4$^{fl/fl}$; K14Cre^{-}) and CerS4$^{epi-/-}$ (CerS4$^{fl/fl}$;K14Cre^{+}) mice at P58. H&E, hematoxylin and eosin; P, postnatal; SG, sebaceous gland.

HFSCs. Indeed, at P58, when CerS4$^{-/-}$ HFs were in anagen, a strong induction of Wnt target gene expression was detected, in line with observations that increased Wnt10b promoted anagen (Li *et al.*, 2013).

Interestingly, downregulation of CerS in *Drosophila* resulted in impaired trafficking of wingless, the *Drosophila* Wnt homolog, and, as a result, a reduction in wingless signaling (Pepperl *et al.*, 2013). This is opposite to our finding in which loss of CerS4 resulted in enhanced Wnt signaling. However, as there is only a single CerS in *Drosophila*, inactivation will strongly reduce ceramide production, whereas loss of CerS4 altered selected ceramide species. How specific ceramide composition of plasma membranes controls BMP and Wnt signaling and/or Wnt expression secretion remains to be resolved. It is well known that lipid composition influences protein activities (Futerman and Hannun, 2004); therefore, the ceramide composition may exert important regulatory functions on the signaling capacity of membrane integral receptors. In this respect, it will be important to determine the lipid composition in HF CerS4^{+} cells to provide further insight into how lipids control BMP and Wnt signaling.

Our data show that CerS4 was localized to different stem/progenitor populations within the HF, such as the JZ, the

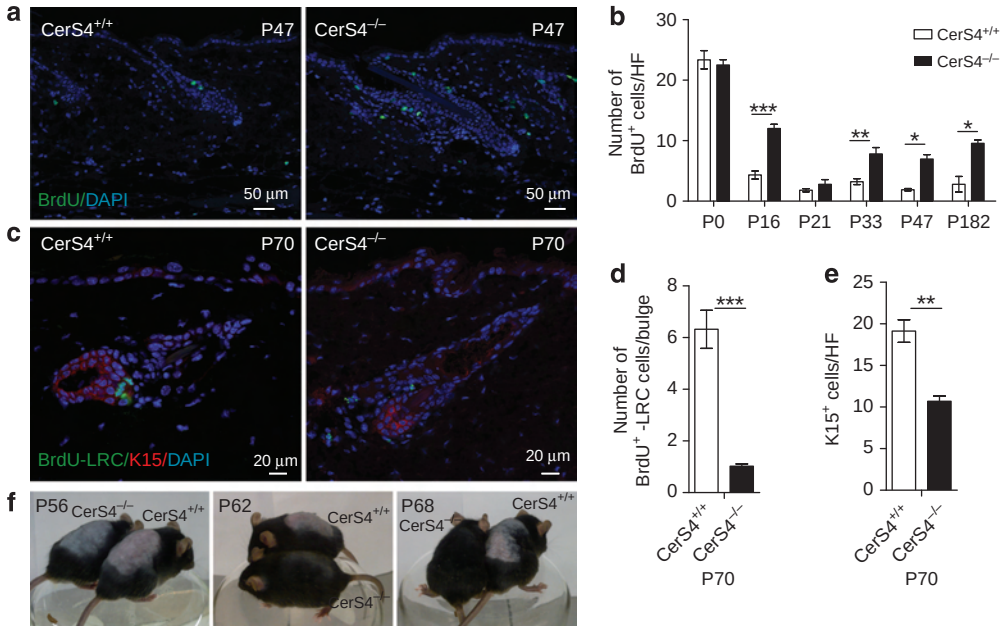

Figure 4. CerS4$^{-/-}$ results in increased proliferation and loss of quiescent bulge stem cells (SC). **(a)** Immunofluorescence staining for BrdU (30 minutes chase) on paraffin sections at P47. **(b)** Quantification of BrdU$^+$ cells in the HF of back skin sections at indicated P days. Mean ± SEM. $n \geq 3$ mice/genotype. *$P<0.05$; **$P<0.01$; ***$P<0.001$. **(c)** Immunofluorescence staining for BrdU-LRC in the K15$^+$ bulge region at P70 after a 58-day challenge. (**a**,**c**) Nuclei were counterstained with DAPI. **(d)** Quantification of BrdU-LRC at P70 in the K15$^+$ bulge region. Mean ± SEM. $n=5$ mice/genotype. ***$P<0.001$. **(e)** Quantification of the number of K15$^+$ cells/HF at P70. Mean ± SEM. $n=5$ mice/genotype. **$P<0.01$. **(f)** Macroscopic appearance at indicated P days after shaving at P47. BrdU, bromodioxyuridine; DAPI, 4',6-diamidino-2-phenylindole; HF, hair follicle; P, postnatal.

isthmus/upper bulge, the hair germ, and to a few cells in the lower bulge of telogen HFs that were only weakly K15$^+$. As α6-integrin$^+$/CD34$^+$ cells were negative for CerS4 mRNA expression, this suggests that these single lower bulge CerS4$^+$ cells are distinct from HFSCs. Which CerS4$^+$ cell compartment is responsible for the precocious activation of HFSCs is not clear. CerS4 in the secondary hair germ or in the isthmus/upper bulge may control cell fate decisions toward follicular or SG differentiation. Alternatively, the single CerS4$^+$ cells in the lower bulge might represent regulatory HFSC niche cells that control HFSC quiescence versus activation.

CerS4 was also highly expressed in the Lrig1$^+$-JZ compartment, and loss of CerS4 resulted in expansion of this domain, as well as SG enlargement. In agreement, a previous study revealed a role for CerS4 in SG homeostasis (Ebel *et al.*, 2014). However, this study did not address the role of CerS4 in other HF compartments. The expansion of the Lrig1$^+$ compartment may be owing to the inappropriate activation of HFSCs that then disproportionally feed into this compartment. Alternatively, CerS4 may directly control the appropriate activity of Lrig1$^+$ progenitors. As Lrig1$^+$ progenitors maintain the infundibulum and the SGs (Page *et al.*, 2013), their expansion may explain the enlargement of the SGs. Importantly, epidermal-specific deletion of CerS4 (CerS4$^{epi-/-}$) recapitulates age-related hair loss and the premature switch of CerS4$^{-/-}$ HFs to anagen, indicating that the regulation of HFSCs is an epidermal-specific CerS4 function and not secondary to systemic or dermal regulatory effects of CerS4 deficiency.

A recent study also showed that loss of CerS4 resulted in age-dependent hair loss (Ebel *et al.*, 2014). However, this was attributed to an increased sebaceous lipid production that obstructed hair shafts, and HFSCs were not examined. Although increased sebaceous lipid production may contribute to hair loss, our study revealed that CerS4 deficiency induced precocious activation of HFSCs and ultimately an almost complete depletion of these bulge SCs, contributing to the age-dependent hair loss in a major way.

In conclusion, we could demonstrate that CerS4-dependent ceramide composition determines adult SC behavior and is essential for a life-long hair coat formation. Because different tissues contain different levels of ceramides with different chain lengths, our data suggest to our knowledge a previously unreported mechanism to tissue-specifically regulate SC activation.

MATERIALS AND METHODS

Mice strains

C57BL/6N mice with floxed CerS4 alleles were generated in cooperation with Taconic Artemis (Cologne, Germany, Supplementary Figure S4 online). To achieve epidermis-specific deletion, CerS4$^{fl/fl}$ mice after Flp deletion were crossed to K14-Cre mice (Hafner *et al.*, 2004). Experiments were performed with CerS4$^{-/-}$ mice, CerS4$^{+/+}$, CerS4$^{fl/fl}$K14Cre$^+$, and CerS4$^{fl/fl}$K14Cre$^-$ littermates at the indicated P days. Mice were kept under specific pathogen-free conditions at the animal facilities of the Medical Centre, University of Cologne. The use of mice was performed according to institutional guidelines and approval by the local authorities of the state North Rhine-Westphalia, in accordance with the animal protection law of Germany.

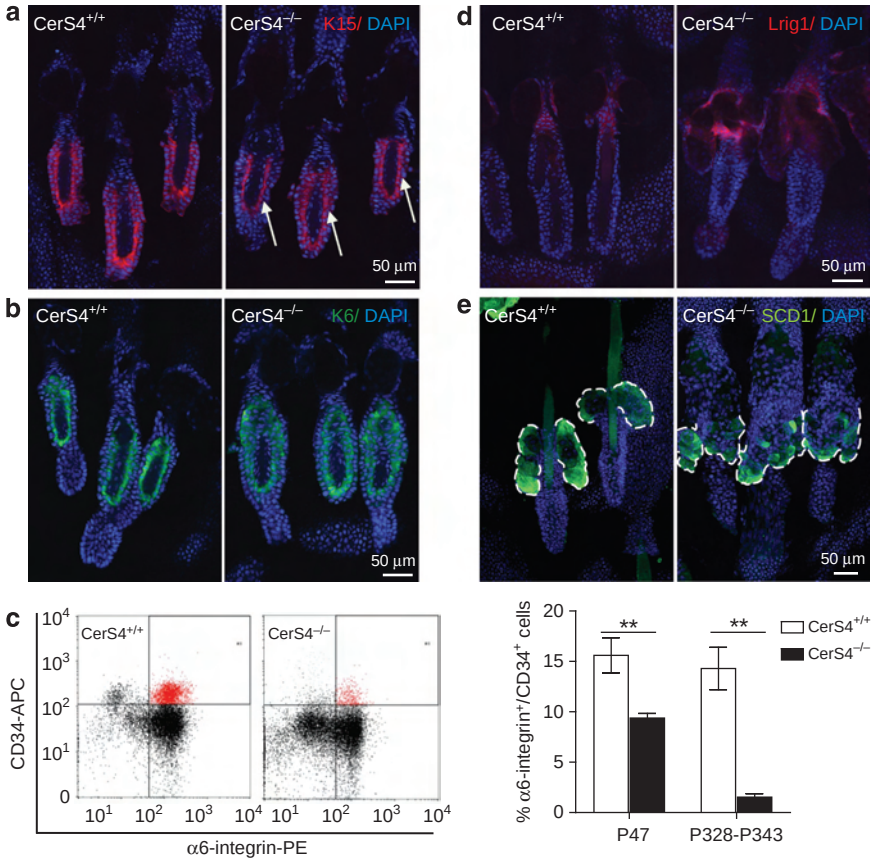

Figure 5. Altered differentiation in epidermal lineages. (**a**,**b**,**d**) Immunohistochemical analysis of K15, K6, and Lrig1 on tail skin whole mounts isolated from CerS4$^{-/-}$ and CerS4$^{+/+}$ mice. Mice were age- and HF phase-matched. White arrows indicate less K15 staining in CerS4$^{-/-}$ whole mounts. Nuclei were counterstained with DAPI. (**c**) FACS analysis (left P328) and quantification (right P47 and P328–P343) of α6-integrin^{+}/CD34^{+} HFSCs from CerS4$^{-/-}$ and CerS4$^{+/+}$ epidermis. Mean ± SEM. $n \geq 3$ mice/genotype. $^{**}P < 0.01$. (**e**) Immunofluorescence staining for SCD1 on tail whole mounts isolated from CerS4$^{-/-}$ and CerS4$^{+/+}$ mice. Dashed line indicates SG area. Nuclei were counterstained with DAPI. DAPI, 4',6-diamidino-2-phenylindole; HF, hair follicle; HFSC, hair follicle stem cell; SG, sebaceous gland.

Tissue collection

Mice were killed and back skin was shaved. For short BrdU-pulse experiments, 25 μg mg^{-1} bodyweight BrdU (Sigma Aldrich, Taufkirchen, Germany) was injected intraperitoneally 30 minutes before scarification. Paraffin and cryosections were prepared as described before (Niessen *et al.*, 2013). The epidermis was separated from the dermis by floating skin biopsies, in a 0.5 M ammonium thiocyanate (NH_4SCN) in phosphate buffer, pH 6.8 (0.1M Na_2HPO_4, 0.1M KH_2PO_4), for 30 minutes on ice.

QRT-PCR

Epidermal RNA was isolated and cDNA was prepared as described before (Niessen *et al.*, 2013). To control for the presence of HF- and IFE-mRNA in epidermal splits, QRT-PCR was performed for K15 and K10 expression (Supplementary Figure S8 online,Supplementary Table 2 online). QRT-PCR for CerS1-6 mRNA expression was performed using the light cycler 480 SYBR Green-I-Master (Roche Applied Sciences, Munich, Germany) with primers for mouse GAPDH (GAPDH-fw: 5′-CATGGCCTCCAAGGAGTAAG3′, GAPDH-rev: 5′-TGTGAGGGAGATGCTCAGTG-3′), CerS1,2,3,5,6 (Schiffmann *et al.*, 2013), and CerS4 (CerS4-fw: 5′-GACCGTGATGGCCTGG TGTT-3′, CerS4-rev: 5′-TCTCCTGATTGGATCCTGCA-3′). Relative quantification of CerS mRNA was calculated using the Pfaffl method (Pfaffl, 2001). QRT-PCR for Wnt- and BMP-signaling pathways was performed using the light cycler 480 noROXMaster Mix (Eurogentec, Seraing, Belgium). For primers, see Supplementary Table 2 online.

Western blot analysis

Epidermal splits were homogenized in 1% SDS and 1 mM EDTA using Precellys 24 Homogenisator (Peqlab, Erlangen, Germany). A measure of 15 μg of protein was separated by SDS-PAGE (Invitrogen, Carlsbad, CA), transferred to polyvinylidene difluoride membranes, and incubated with primary and secondary antibodies (Supplementary Table 3 online). Antibody binding was visualized using SuperSignal West Pico Chemiluminescent substrate (34078, Thermo Scientific, Rockford, IL).

For ceramide analysis and ceramide synthase activity assay, see Supplementary Materials and methods

Immunohistochemistry and isolation of tail skin whole mounts. Paraffin sections and cryosections were used for immunohistochemistry, as described before (Niessen *et al.*, 2013). Briefly, sections were incubated for 3 hours with primary antibodies

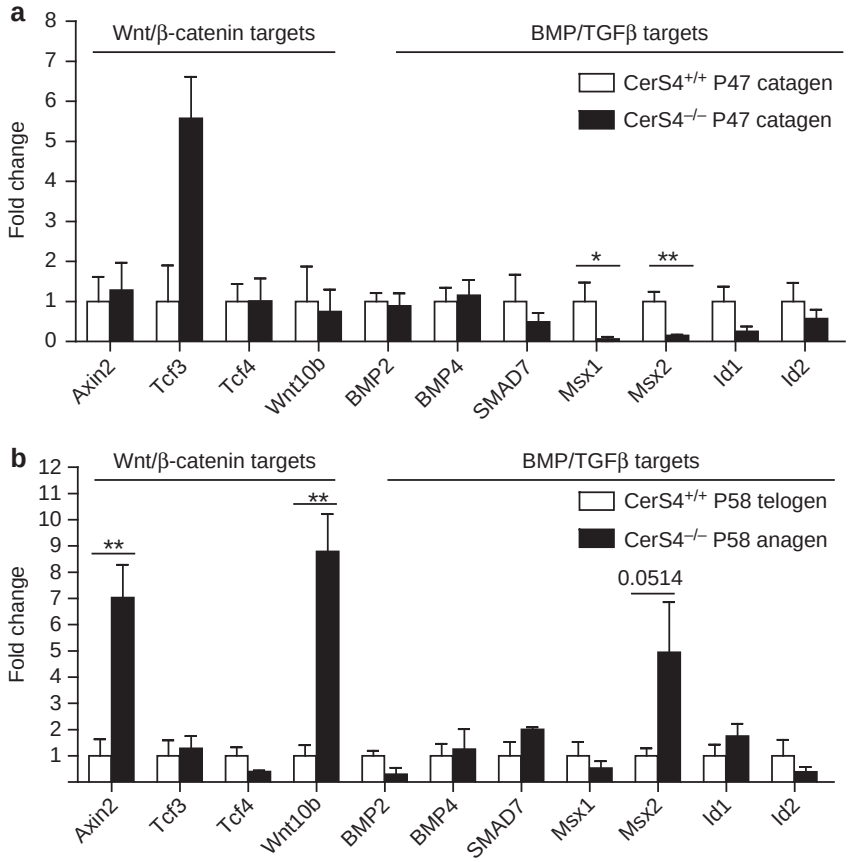

Figure 6. Decreased BMP (P47) and increased Wnt (P58) mRNA expression in CerS4$^{-/-}$ epidermis. QRT-PCR analysis of Wnt and BMP target genes: *Axin2, Tcf3, Tcf4, Wnt10b, BMP2, BMP4, Smad7, Msx1, Msx2, Id1*, and *Id2* of epidermal splits isolated from CerS4$^{-/-}$ and CerS4$^{+/+}$ mice at (**a**) P47 and (**b**) P58. Values of CerS4$^{-/-}$ mRNA expression were normalized to CerS4$^{+/+}$ (CerS4$^{+/+}$ = 1). Mean ± SEM of $n \geq 3$ mice/genotype, *$P<0.05$, **$P<0.01$. BMP, bone morphogenetic protein; Wnt, Wg for wingless and Int for the Int-gene; QRT-PCR, quantitative real-time PCR.

(Supplementary Table 3 online) diluted in blocking solution, followed by incubation with the secondary antibody (Supplementary Table 3 online) for 1 hour at room temperature. Nuclei were counterstained using DAPI (4',6-diamidino-2-phenylindole; Sigma Aldrich).Tail skin whole mounts were prepared as previously described (Muller-Rover *et al.*, 2001; Niessen *et al.*, 2013).

BrdU label–retaining experiment. Ten-day-old mice were injected with BrdU (see above) every 24 hours for three injections (P10–12). After a 58-day chase period (Braun *et al.*, 2003), the dorsal skin was isolated for analysis.

FACS analysis

FACS analysis was performed as described previously (Niessen *et al.*, 2013). Subsequent analysis was performed using FACSCanto II (BD, Heidelberg, Germany) equipped with the BD Diva software or FACSCalibur (BD) equipped with BD CellQuest Pro.

Hair regrowth

The back skin of P47 (catagen) mice was shaved with an electric shaver under general anesthesia. Hair growth was documented daily by photographs for 3 weeks.

Image acquisition

Hematoxylin and eosin (H&E) stainings were analyzed via light microscopy using Olympus (Hamburg, Germany) BX51. Fluorescent stainings were analyzed using an Olympus IX71, a confocal microscope Zeiss (Oberkochen, Germany) Meta 510, with a confocal Olympus FV1000 microscope, or a TCS SP8 gSTED, Leica (Wetzlar, Germany) Confocal laser scanning microscope.

Statistical analysis

To analyze statistical significance, the unpaired Student's *t*-test was performed. **P*-values <0.05 ; **$P<0.01$; ***$P<0.005$ were considered statistically significant.

CONFLICT OF INTEREST

The authors state no conflict of interest.

ACKNOWLEDGMENTS

We thank U. Karow, K. Kroll, A. Schmitz, S. Schramm, and S. Moll for valuable experimental help and B. Eckes for help with the light microscopy. We acknowledge the help of the central FACS facility, especially G. Rappel of the CMMC. Furthermore, we acknowledge the help of the Central Imaging Facility of CECAD. We also thank M. Fink and O. Utermöhlen for discussion and the helpful input. CMN, JCB, and MK are supported by the DFG (SFB 670, SFB829, and SFB832) and Deutsche Krebshilfe.

SUPPLEMENTARY MATERIAL

Supplementary material online is linked to the online version of the paper at

http://www.nature.com/jid

REFERENCES

Alonso L, Fuchs E (2006) The hair cycle. *J Cell Sci* 119:391–3

Blanpain C, Fuchs E (2009) Epidermal homeostasis: a balancing act of stem cells in the skin. *Nat Rev Mol Cell Biol* 10:207–17

Braun KM, Niemann C, Jensen UB *et al.* (2003) Manipulation of stem cell proliferation and lineage commitment: visualisation of label-retaining cells in wholemounts of mouse epidermis. *Development* 130:5241–5

Claxton JH (1966) The hair follicle group in mice. *Anat Rec* 154:195–207

Ebel P, Imgrund S, Vom Dorp K *et al.* (2014) Ceramide Synthase 4 deficiency in mice causes lipid alterations in sebum and results in alopecia. *Biochem J* 461:147–58

Fuchs E, Chen T (2013) A matter of life and death: self-renewal in stem cells. *EMBO Rep* 14:39–48

Futerman AH, Hannun YA (2004) The complex life of simple sphingolipids. *EMBO Rep* 5:777–82

Goldstein J, Horsley V (2012) Home sweet home: skin stem cell niches. *Cell Mol Life Sci* 69:2573–82

Greco V, Chen T, Rendl M *et al.* (2009) A two-step mechanism for stem cell activation during hair regeneration. *Cell Stem Cell* 4:155–69

Hafner M, Wenk J, Nenci A *et al.* (2004) Keratin 14 Cre transgenic mice authenticate keratin 14 as an oocyte-expressed protein. *Genesis* 38:176–81

Hartmann D, Wegner MS, Wanger RA *et al.* (2013) The equilibrium between long and very long chain ceramides is important for the fate of the cell and can be influenced by co-expression of CerS. *Int J Biochem Cell Biol* 45: 1195–203

Hsu YC, Pasolli HA, Fuchs E (2011) Dynamics between stem cells, niche, and progeny in the hair follicle. *Cell* 144:92–105

Imokawa G, Abe A, Jin K *et al.* (1991) Decreased level of ceramides in stratum corneum of atopic dermatitis: an etiologic factor in atopic dry skin? *J Invest Dermatol* 96:523–6

Jennemann R, Rabionet M, Gorgas K *et al.* (2012) Loss of ceramide synthase 3 causes lethal skin barrier disruption. *Hum Mol Genet* 21:586–608

Jensen KB, Collins CA, Nascimento E *et al.* (2009) Lrig1 expression defines a distinct multipotent stem cell population in mammalian epidermis. *Cell Stem Cell* 4:427–39

Kandyba E, Leung Y, Chen YB *et al.* (2013) Competitive balance of intrabulge BMP/Wnt signaling reveals a robust gene network ruling stem cell homeostasis and cyclic activation. *ProcNatl Acad Sci USA* 110:1351–6

Kobielak K, Stokes N, de la Cruz J *et al.* (2007) Loss of a quiescent niche but not follicle stem cells in the absence of bone morphogenetic protein signaling. *Proc Natl Acad Sci USA* 104:10063–8

Laviad EL, Albee L, Pankova-Kholmyansky I *et al.* (2008) Characterization of ceramide synthase 2: tissue distribution, substrate specificity, and inhibition by sphingosine 1-phosphate. *J Biol Chem* 283:5677–84

Levy M, Futerman AH (2010) Mammalian ceramide synthases". *IUBMB Life* 62: 347–56

Li YH, Zhang K, Yang K *et al.* (2013) Adenovirus-mediated Wnt10b overexpression induces hair follicle regeneration. *J Invest Dermatol* 133: 42–8

Maceyka M, Spiegel S (2014) Sphingolipid metabolites in inflammatory disease. *Nature* 510:58–67

Mizutani Y, Kihara A, Igarashi Y (2005) Mammalian Lass6 and its related family members regulate synthesis of specific ceramides. *Biochem J* 390: 263–71

Muller-Rover S, Handjiski B, van der Veen C *et al.* (2001) A comprehensive guide for the accurate classification of murine hair follicles in distinct hair cycle stages. *J Invest Dermatol* 117:3–15

Niessen MT, Scott J, Zielinski JG *et al.* (2013) aPKClambda controls epidermal homeostasis and stem cell fate through regulation of division orientation. *J Cell Biol* 202:887–900

Page ME, Lombard P, Ng F *et al.* (2013) The epidermis comprises autonomous compartments maintained by distinct stem cell populations. *Cell Stem Cell* 13:471–82

Pepperl J, Reim G, Luthi U *et al.* (2013) Sphingolipid depletion impairs endocytic traffic and inhibits Wingless signaling. *Mech Dev* 130:493–505

Pettus BJ, Chalfant CE, Hannun YA (2002) Ceramide in apoptosis: an overview and current perspectives. *Biochim Biophys Acta* 1585:114–25

Pfaffl MW (2001) A new mathematical model for relative quantification in real-time RT-PCR. *Nucleic Acids Res* 29:e45

Plikus MV, Baker RE, Chen CC *et al.* (2011) Self-organizing and stochastic behaviors during the regeneration of hair stem cells. *Science* 332:586–9

Plikus MV, Mayer JA, de la Cruz D *et al.* (2008) Cyclic dermal BMP signalling regulates stem cell activation during hair regeneration. *Nature* 451: 340–4

Rabionet M, Gorgas K, Sandhoff R (2014) Ceramide synthesis in the epidermis. *Biochim Biophys Acta* 1841:422–34

Schiffmann S, Birod K, Mannich J *et al.* (2013) Ceramide metabolism in mouse tissue. *Int J Biochem Cell Biol* 45:1886–94

Schwenk F, Baron U, Rajewsky K (1995) A cre-transgenic mouse strain for the ubiquitous deletion of loxP-flanked gene segments including deletion in germ cells. *Nucleic Acids Res* 23:5080–1